Growth of Sb_2Te_3 thin films on Ge(111) sample by thermal deposition: Morphological and electronic properties

Marco Minissale, Eric Salomon, Konstantinos Iliopoulos, Julien Lumeau, Thierry Angot

Growth of Sb_2Te_3 thin films on Ge(111) sample by thermal deposition: morphological and electronic properties

Marco Minissale[a], Eric Salomon[a], Konstantinos Iliopoulos[b], Julien Lumeau[b], Thierry Angot[a]

[a]*Aix Marseille Univ, CNRS, PIIM, France,*
[b]*Aix Marseille Univ, CNRS, Centrale Med, Institut Fresnel, Marseille, France,*

Abstract

Sb_2Te_3 is a well-known thermoelectric material and a topological insulator and its utilization is foreseen for many applications, such as quantum computing, mode-locking of laser systems, and cooling systems.
Various methods have been used to grow thin Sb_2Te_3 films on different substrates, such as molecular beam epitaxy or electrodeposition. Often, such methods require performing laborious and rigid steps in order to optimize film growth and reduce the amount of defects.
For this reason, we investigate a simplified growth method: thermal deposition starting from Sb_2Te_3 lumps followed by annealing. By means of various surface science techniques (LEED, STM, XPS), we show that it is possible to obtain a single crystalline Sb_2Te_3 film on a Ge(111) substrate.
The film, which is amorphous after deposition, undergoes a phase transition and becomes crystalline after annealing at 573 K. This is clearly shown by a 1x1 surface termination typical of a (0001) surface with hexagonal lattices. The presence of several quintuple-layer steps was observed by scanning tunneling microscopy. Photoelectron spectroscopy characterization confirms that the grown chalcogenide film presents the expected stoichiometry (Te/Sb=1.5).
The proposed method simplifies the growth phase and seem to reduce the number of defects induced by the growth technique, major advantages for many applications.

Keywords: Antimony telluride, Germanium, Thin film growth, Morphology, Topological insulator
PACS: 0000, 1111
2000 MSC: 0000, 1111

1. Introduction

X_2Y_3 (X=Bi, Sb; Y= Se, Te) are chalcogenide compounds with a narrow gap and a rhombohedral crystalline structure. The structure consists of atoms covalently bonded by van der Waals attraction to form 5 atom thick layers (in order: Y-X-Y-X-Y),), commonly referred as quintuple layers (QLs). Such materials have high thermoelectric efficiency [1], which allows them to convert heat directly into electricity making them suitable for cooling applications [2].

More recently, X_2Y_3 compounds have attracted a major interest due to their unique electronic band structure which causes them to conduct electricity on their surface but not in their interior [3, 4, 5]. This can be considered as a new state of matter known as a three-dimensional (3D) "topological insulator" that has potential applications in spintronics and quantum computing [6, 7, 8, 9].

Moreover, X_2Y_3 films exhibit non-linear optical properties suitable for super-resolution and mode-locking of laser systems [10, 11, 12].

For all these reasons, an increasing number of researches deals with their growth on different substrates, Si(111) [13, 14, 15], Ge(111) [16], SiO_2 [17], GaAs(111) [18], just to mention a few.

In the case of Sb_2Te_3, various methods have been used, including solid state reaction route [19], electrodeposition [20], catalyst-free vapor-solid [17], RF-magnetron sputtering [21], atomic layer deposition [22], molecular beam epitaxy (MBE) [18, 23, 24], metal–organic chemical vapor deposition [15]. All these techniques have shown promising results, but often finding the optimized growth recipe can be very laborious. As pointed out by Liu et al. [13], in the case of Bi_2Te_3 grown by MBE, a good layer-by-layer structure is formed only under optimal conditions, with the Te/Bi flux ratio that controls the growth rate, but also the clustering and the amount of defects. Similarly, in the case of metal–organic chemical vapor deposition, it has been shown that the quality of Sb_2Te_3 films grown on silicon depends on both the precursors vapor pressures and the total flow [15]. Since the implementation into electronics and spintronic devices requires for thin and, as far as possible, defect-free film structures, it is mandatory to reduce the amount of defects induced by growth technique [23]. Here we investigate the possibility to grow thin film using a simplified method: thermal deposition starting from Sb_2Te_3 lumps followed by annealing.

Recently we have shown that films prepared using this method exhibit significant nonlinear optical properties [11]. Nevertheless, the morphological and stoichiometric properties

of resulting chalcogenide films have not been fully characterized. To gain insight into such properties, a systematic study was conducted using typical surface science techniques: low-energy electron diffraction (LEED), X-ray photoelectron spectroscopy (XPS) and scanning tunneling microscopy (STM). The growth was performed on a Ge(111) substrate. This system has not been yet studied, contrarily to Sb_2Te_3 on Si(111), despite some possible intrinsic advantages: Sb_2Te_3 should have a smaller lattice mismatch with Ge(111) (6%) than with Si(111) (11%) which should prevent from defects induced by strain and lattice mismatch.

2. Methods

Sample preparation and analysis were performed using an ultra-high vacuum (base pressure: 10^{-8} Pa) setup composed of four interconnected chambers equipped, respectively, with

1. cleaning and preparation facilities: an ion source ISE-10 Scienta Omicron, a home-made heating system, an e-beam evaporator EFM-3T Scienta-Omicron and a LEED apparatus (Scienta-Omicron);
2. a variable-temperature STM (Scienta-Omicron);
3. a high-resolution electron energy loss spectrometer (HREELS) (DELTA0.5);
4. a photoelectron spectroscopy (XPS and UPS) facility: a non-monochromatized Mg X-ray source emitting at 1253.6 eV (Kα) (PREVAC), an UV source (HIS13, Scienta-Omicron) using He I (hν = 21.22 eV), a R3000 Electron Spectrometer equipped with a MCP detector and a CCD camera allowing angular-resolved (AR) measurements (Scienta-Omicron). The resolution in XPS measurements, determined from the FWHM of Ag 3d core levels, recorded on the clean surface, was 0.8 eV [25]. The resolution in UPS, evaluated from the Fermi step recorded on a Mo foil nearby the sample, is about 0.15 eV.

Prior to chalcogenide film growth, the Ge(111) substrate was prepared as described in Minissale et al. [26]: several cycles of Ar^+ ion bombardment at 1500 eV at room temperature (RT) followed by annealing at 900 K and a slow cooling phase (0.25 K/s). The preparation of the Ge(111) substrate was performed until a c(2×8) LEED pattern was clearly identified (Fig. 1, left panel). Chalcogenide film growth is usually performed using different crucibles for each species and changing the crucibles temperature depending on the species and its sublimation temperature. Sb_2Te_3 thin films growth was studied by Plucinski et al. [23] using effusion cell temperatures of 723 K and 590 K for Sb and Te, respectively. As already presented before, in this work we adopted a different growth method: a Sb_2Te_3 lump (~ 6 mm^3, CODEX International 99,99%) was placed in an outgassed molybdenum-crucible and heated to around 670 K[1]. The pressure raised up to 3×10^{-7} Pa during thermal evaporation. The atomically clean substrate was held at RT during deposition. Subsequently, the film/substrate was heated to 573±20 K to induce crystallization of the deposited film, as discussed elsewhere [11, 12]. We highlight that we performed several thermal depositions (varying the evaporation time from 3 to 15 minutes) to test how the thickness can influence the film properties (amorphous-crystalline transition, stoichiometry, ...). We will focus mainly on the results obtained after 6 minutes of evaporation, even if slight variations of the film properties were observed (e.g. thickness).

[1] We stress that we did not directly measure the temperature of the crucible but we extracted it from the EFM-3T evaporator calibration curves.

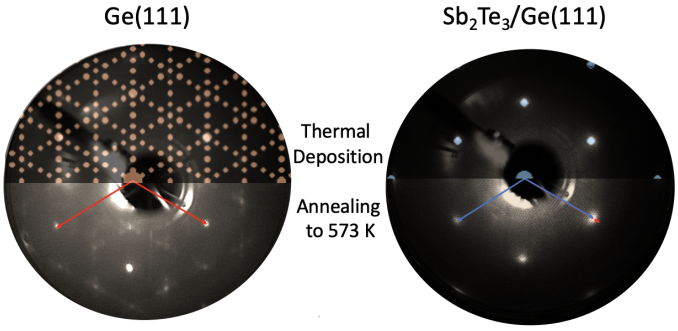

Figure 1: LEED patterns recorded at 58 eV on the clean Ge(111) substrate (left) and on the Sb_2Te_3 film grown on Ge(111) and annealed at 573±20 K. Red and blue arrows represent the unit vectors of the 1x1 reconstructions of the Ge and Sb_2Te_3 surfaces, respectively. The simulated surface reconstructions are superimposed on the LEED experimental patterns. The simulation does not compute spot intensities, but only the structural model.

3. Results and discussion

The analysis of the surface structure of the film was performed using LEED. As already mentioned, the clean Ge(111) presents a typical c(2×8) surface reconstruction. The left panel of Fig. 1 shows experimental and simulated LEED pattern of the Ge(111). We pinpoint that the simulated LEED pattern was obtained using *LEEDpat* software, it does not compute spot intensities, but only the structural model. The red arrows represent the unit vectors of the 1×1 reconstruction of Ge surface. After thermal deposition of Sb_2Te_3 film, such reconstruction disappears and only a diffuse pattern is observed indicating the presence of an amorphous chalcogenide phase. After the annealing to 573 K a LEED pattern is again visible (right panel in Fig. 1), suggesting an amorphous-crystalline phase transition of the film. On the figure, blue arrows represent the unit vectors of the Sb_2Te_3 diffraction pattern. By comparing the length of such vectors (blue and red), we measure a difference of 7.2±1.5 % between the lattice vectors of the Sb_2Te_3 film with respect to the (1x1) lattice vectors of Ge(111). This value is in good agreement with 6.5%, the difference between the lattice constant of the two bulk materials (4.26 and 4.00 Åfor Sb_2Te_3 and Ge, respectively). We underline that such a mismatch could nevertheless favor the presence of defects (e.g. dislocations) [18] and explain the (relatively) large diffraction spots observed in the case of Sb_2Te_3 film.

The evolution of the Te/Sb stoichiometry for the different epitaxial growths and during annealing was studied using photoelectron spectroscopy. XPS studies are often focused on Te

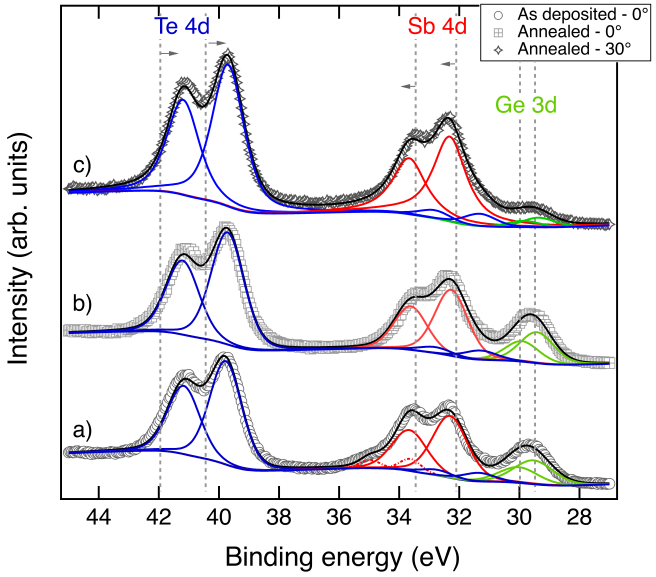

Figure 2: Te 4*d*, Sb 4*d* and Ge 3*d* core levels obtained on a Sb_2Te_3 film deposited on Ge(111): a) after evaporation for an emission angle of 0° with respect to the surface normal; b) after annealing at 573 K for an emission angle of 0° with respect to the surface normal; c) after annealing at 573 K for an emission angle of 30° with respect to the surface normal. The solid curves represent the fit of the experimental data. Dashed gray lines show the binding energy for the pure element core levels.

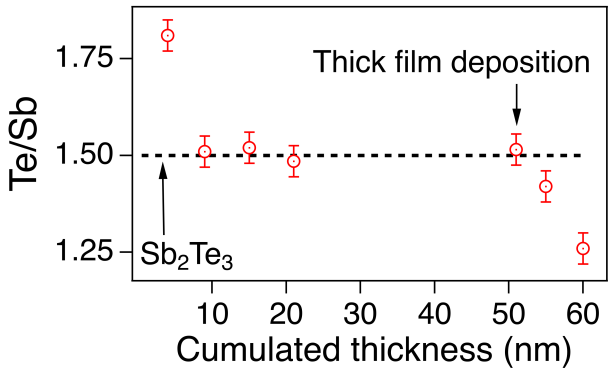

Figure 3: Stoichiometry evolution evaluated using X-ray photoelectron spectroscopy for different film of Sb_2Te_3 grown on Ge(111) using the same lump. The stoichiometry has been evaluated after annealing at 573 K.

3*d* and Sb 3*d* core levels (CLs), in the 585-525 binding energy (BE) range, since they exhibit the highest photoionization cross-sections when using Mg-Kα source. Although we have systematically recorded Te 3*d* and Sb 3*d* core levels, in this work we decided to perform the XPS analysis rather in the 44-28 eV BE region, in order to simultaneously detect Te 4*d*, Sb 4*d* and Ge 3*d*. This choice is somewhat constrained by the partial overlap of Sb 4*d* and Ge 3*d*.

On the other hand, the use of a short BE range allows to minimize the difference in the escape depth of the photoelectrons produced by Te, Sb and Ge. This appears to be a key factor for an optimal determination of the film thickness as we will show later. Fig. 2 shows an example of XPS spectra measured after growth of the film at 300 K (a) and after annealing at 573 K (b and c). The BE of the peaks in both spectra, 38.7 eV (41.2 eV) for Te $4d_{5/2}$ ($4d_{3/2}$), 32.3 eV (33.6 eV) for Sb $4d_{5/2}$ ($4d_{3/2}$) and 29.6 eV for Ge 3*d*, where the doublet induced by the spin-orbit coupling is not resolved. Compared to pure elements, a clear red shift (-0.55±0.10 eV) for Te 4*d* and a blue shift (0.35±0.10 eV) for Sb 4*d* can be observed on the figure [27, 28]. Comparable shifts were observed for the Te 3*d* and Sb 3*d* CLs. Similarly to what is claimed by Kim et al. [16] for Bi_2Se_3 grown on Ge(111), the observed chemical shift should be due to electron charge transfer from Sb to Te giving rise to Sb^{3+} and Te^{2-} chemical states in the Te-Sb bonds. The BE and the intensity of each components was estimated using the fit shown by solid lines in Fig. 2. The present fit was obtained using a Shirley background and Voigt profiles by fixing the width to 1.3 eV and the Gaussian/Lorentz (GL) ratio to 0.35 for all peaks. We stress that the width was varied between 1.15 and 1.35 eV and GL ratio between 0.3 and 0.5. Varying such parameters influences only slightly the intensity (< 3%) and the position (< 0.2%) of the peaks, therefore we decided to fix to the values (GL=0.3, width=1.3 eV) which provide the best fit. Thus the only free parameters are the area and the position of peaks.

Let us mention that in addition to the previously listed CLs of Te, Sb and Ge, we also detected supplementary peaks. A first doublet around 32 eV is due to the satellite Mg K_{α_3} line (relative intensity 8% with respect to $K_{\alpha_{1,2}}$) that induces a shift of 8.4 eV in the kinetic energy of photoelectrons from Te 4*d*, and thus in the "apparent" BE. We pinpoint that the fit was performed by fixing the intensity (8%) and the position (-8.4 eV) of such doublet with respect to the Te 4*d* at 42-39 eV. A second doublet is present at about 35 eV after evaporation (Fig. 2a) and it has been assigned to Sb 4*d*, probably due to dangling Sb atoms or an oxidized state [28]. This doublet disappears after annealing at 573 K. The fit has been used to evaluate the ratio between Te and Sb, its evolution as a function of temperature and for different film growths (Fig. 3). Just after deposition the ratio Te/Sb_{total} is 1.63±0.04 while it is 1.33±0.04 if only the main Sb 4*d* doublet is considered. After annealing the ratio becomes 1.48±0.04, in agreement with the theoretical value (1.5). Furthermore, we point out that increasing the annealing temperature above 600 K can result in a Te-depleted film and to a complete desorption of the film for temperatures higher than 650 K. We stress that after annealing the only parameters that change in the case of Sb 4*d* CLs are the peak intensities. This suggests that a part of Sb atoms responsible of the doublet at 35 eV are actually included in the main Sb 4*d* CL after annealing. Fig. 3 shows the evolution of the stoichiometry, evaluated after annealing at 573 K, for different growths using the same lump of Sb_2Te_3. One can note that the film is richer in Te for the first growth and depleted in Te for the last growths. This can be explained by the different melting temperatures of Sb and Te (904 and 723 K): it may favor an initial sublimation of Te giving rise to a Te-rich film. The Te-depleted films after many depositions are a direct consequence of the initial Te-rich film. We pinpoint that no LEED pattern was observed in non-stoichiometric films,

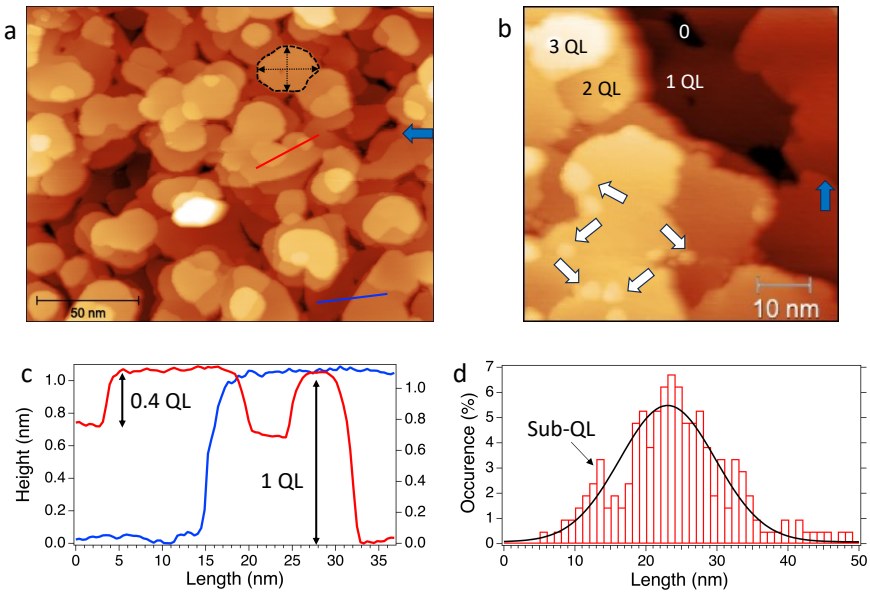

Figure 4: STM images (*a* and *b*) of Sb_2Te_3 film of 4.3 nm grown on Ge(111) acquired at 300 K. The tunneling parameters are in the range U_{sample}=2-3 V, I_t=0.2-0.3 nA. The possible presence of dislocation cores is indicated by blue arrows. In *b* the step height is given in quintuple layers (QLs) with respect to the plane called "0". Sub-QL islands are depicted with white arrows.The profiles along red and blue lines are shown in the height profile *c*. The *d* shows the grain size distribution averaged over 100 grains considering two lengths per grain as shown in panel *a*. The gaussian distribution is centered at 23±9 nm. The high occurrence around 10 nm is given to sub-QL islands.

indicating the lack of crystallinity.

We also point out that after the first deposition, it is possible to obtain films of the desired thickness with a ratio of about 1.5. We emphasize that although there is an obvious relationship between the volume of the initial Sb_2Te_3 lump and the maximum thickness that can be grown, the cumulative thickness shown in Fig. 3 is also strongly influenced by the distance between the effusion cell and the substrate. In our case, the distance of about 20 cm and the shape of the crucible are not optimized to maximize the deposition on the substrate and thus to minimize the loss of the material due to pumping.

XPS was used also to estimate the thickness of the chalcogenide film by varying the angle of detection with respect to the surface normal (Fig. 2b and c) and by carrying out a Strohmeier analysis [29] based on the following equation:

$$d = \lambda_f \cdot sin\theta \cdot ln(\frac{N_s \cdot \lambda_s \cdot I_f}{N_f \cdot \lambda_f \cdot I_s} + 1) \quad (1)$$

where the $\lambda_{f,s}$ are the the inelastic mean free paths (IMFPs) of the photoelectrons in the film (λ_s=2.57 nm) and the substrate (λ_s=2.21 nm), $N_{f,s}$ the volume densities of the film (6.5 g·cm^{-3}) and the substrate (5.3 g·cm^{-3}), θ the electron take-off angle (with respect to the sample surface), I_f and I_f the intensity of the film and the substrate, respectively. Here, I_f has been calculated as the sum of the Te and Sb intensity. The thickness was estimated to be about 4.3±1.2 nm, or rather, 4 quintuple layers (QLs), where each QL consists of Te–Sb–Te–Sb–Te atomic layers of 1.01 nm [24].

Further information about the surface topography are obtained by STM images shown in Fig. 4. STM data are acquired at 300 K and the tunneling parameters are in the range U_{sample}=2-3 V, I_t=0.2-0.3 nA. From the large-scale STM image shown in Fig. 4a, we can observe the presence of terraces with a typical size of 23±9 nm (Fig. 4d). Such flat terraces are separated from each other by steps of 1.04±0.03 nm, as presented in the height profile in Fig. 4c. In Fig. 4b, it is also possible to observe the presence of sub-QL islands indicated by white arrows. The sub-QL islands present a thickness of 0.4 QL (red line in Fig. 4c), as already measured by Lanius et al. [24] in the case of Sb_2Te_3 on Si(111) by MBE. The typical size of such sub-QL islands is of 10 nm as shown in the grain distribution (Fig. 4d). Moreover, only few dislocations, marked by blue arrows, are visible in our film contrarily to the rich variety of morphological structures (e.g. screw dislocations, antiphase-like defects) observed by Lanius et al. Finally, UPS measurements recorded at room-temperature on a freshly grown sample are shown in Fig. 5. The overall aspect of the spectrum is in good agreement with data from the literature and reproduces the various low binding energy components labeled β, γ, δ, and ϵ observed on both cleaved crystals and Sb_2Te_3 films grown by MBE [23, 30, 31]. The main difference with the UPS data in the literature is the absence the lowest B.E. component labeled α. This can be explained by several factors: first, the thickness of our film (about 4 QL) is smaller than all other films reported elsewhere, resulting in less pronounced features. In addition, the presented spectrum is integrated over the whole detector to obtain a good signal-to-noise ratio, i.e. over a *k*-space ranging from -0.36 to +0.36 Å^{-1}. This large integration range tends to reduce the spectral weight of the α component relative to the others. Therefore, we expect the spectrum to be more like the one presented by C. Pauly et al. when centered at 0.26 Å^{-1}[30]. Also, it should also be mentioned that the small

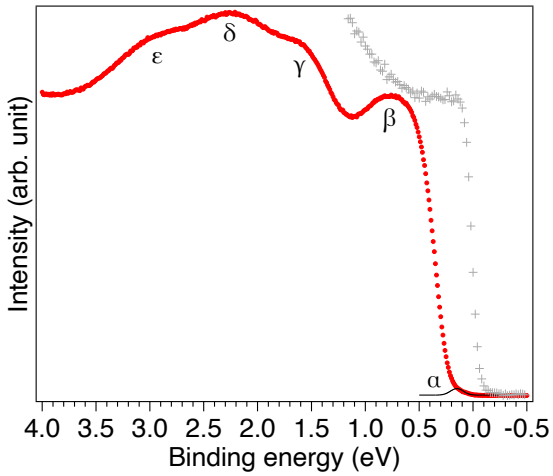

Figure 5: Integrated UPS spectra recorded on a freshly grown 4 QL thick film of Sb_2Te_3 (full-circle) and on a Mo foil nearby (cross). The features labeled α, β, γ, δ, and ϵ refer to similar components reported elsewhere [23].

grain size and thus the associated joint grain density of our film may contribute to a low spectral weight of the α component. Nevertheless, considering the steepness of the decreasing slope towards 0 eV B.E., which is softer than that of the Fermi level (gray dots in Fig. 5), one can intuit the presence of a certain density of states which can be related to the α component, as represented by the black curve in Fig. 5.

4. Conclusions

In summary, we have shown how single crystalline Sb_2Te_3 thin films can be grown on a Ge(111) substrate directly from thermal evaporation of Sb_2Te_3 lumps. The film is amorphous after deposition and undergoes a phase transition to become crystalline after annealing at 573 K. This is clearly shown by the 1x1 surface termination typical of a (0001) surface with hexagonal lattices with quintuple-layer steps. The presence of several QLs steps was observed by scanning tunneling microscopy together with the presence of some sub-QL regions. XPS characterization allows to confirm that the grown chalcogenide film has the expected stoichiometry (Te/Sb~1.5), except for the first grown film, and after several growths (more than 50 nm).

As suggested by Kim et al. [16] in the case of Bi_2Se_3, the Sb_2Te_3 film grown on Ge(111) is expected to have a sharper interface than that on Si(111), studied elsewhere [24], due to the smaller lattice mismatch between the two materials, and thus, to be more suitable for device applications. On the other hand, it is not known how the lattice mismatch induced by Ge(111) modifies the band structure of the growth film and whether the material can still be considered as a topological insulator. For this reason, we plan in the future to characterize the band structure of such films using synchrotron radiation and angle-resolved photoelectron spectroscopy. Such measurements could also provide insight into the reasons for the unclear detection of the α component in the UPS spectrum.

Moreover, from an application point of view, it is important to understand how morphological and electronic properties of grown films evolve as a function of time in air. The methodology used in this work will be coupled with Raman spectroscopy to determine the possible presence of non-stoichiometric islands and to study the aging of the film. Eventually, we will test if such growth method can be extended to other films (e.g. Bi_2Te_3 or Bi_2Se_3 /Ge(111)), other orientations (Ge(110)) that should allow the formation of elongated structures of chalcogenide, or even other substrates (e.g. Bi) that present a smaller mismatch (4.33 Å).

References

[1] N. Peranio, O. Eibl, J. Nurnus, Structural and thermoelectric properties of epitaxially grown Bi_2Te_3 thin films and superlattices, Journal of Applied Physics 100 (11) (2006) 114306. doi:10.1063/1.2375016.

[2] A. Raja, R. M. Jauhar, K. Ramachandran, S. Vediyappan, R. Kumar Raji, M. S. Pandian, R. Perumalsamy, A quintuple-layered binary chalcogenide Sb_2Te_3 single crystal and its transport properties for thermoelectric applications, ACS Omega 7 (32) (2022) 27798–27803. doi:10.1021/acsomega.1c05972.

[3] H. Zhang, C.-X. Liu, X.-L. Qi, X. Dai, Z. Fang, S.-C. Zhang, Topological insulators in Bi_2Se_3, Bi_2Te_3 and Sb_2Te_3 with a single Dirac cone on the surface, Nature Physics 5 (6) (2009) 438–442. doi:10.1038/nphys1270.

[4] J. Zhang, C.-Z. Chang, Z. Zhang, J. Wen, X. Feng, K. Li, M. Liu, K. He, L. Wang, X. Chen, Q.-K. Xue, X. Ma, Y. Wang, Band structure engineering in $(Bi_{1-x}Sb_x)_2Te_3$ ternary topological insulators, Nature Communications 2 (1) (2011) 574. doi:10.1038/ncomms1588.

[5] L. Locatelli, A. Kumar, P. Tsipas, A. Dimoulas, E. Longo, R. Mantovan, Magnetotransport and ARPES studies of the topological insulators Sb_2Te_3 and Bi_2Te_3 grown by MOCVD on large-area Si substrates, Scientific Reports 12 (1) (2022) 3891. doi:10.1038/s41598-022-07496-7.

[6] J. Moore, The birth of topological insulators, Nature 464 (2010) 194–198. doi:10.1038/nature08916.

[7] E. Longo, M. Belli, M. Alia, M. Rimoldi, R. Cecchini, M. Longo, C. Wiemer, L. Locatelli, P. Tsipas, A. Dimoulas, G. Gubbiotti, M. Fanciulli, R. Mantovan, Large spin-to-charge conversion at room temperature in extended epitaxial Sb_2Te_3 topological insulator chemically grown on silicon, Advanced Functional Materials 32 (4) (2022) 2109361. doi:https://doi.org/10.1002/adfm.202109361.

[8] S. Teresi, N. Sebe, J. Patterson, T. Frottier, A. Kandazoglou, P. Noël, P. Sgarro, D. Térébénec, N. Bernier, F. Hippert, J.-P. Attané, L. Vila, P. Noé, M. Cosset-Chéneau, Spin-orbit readout using thin films of topological insulator Sb_2Te_3 deposited by industrial magnetron sputtering, Advanced Functional Materials 33 (44) (2023) 2303878. doi:https://doi.org/10.1002/adfm.202303878.

[9] R. Kumar, P. Bajracharya, P. Haghi Ashtiani, R. Paxson, R. Kolagani, R. C. Budhani, Planar hall effect and magnetoresistance of Sb_2Te_3 epitaxial films, Phys. Rev. B 109 (2024) 075421. doi:10.1103/PhysRevB.109.075421.

[10] J. Sotor, G. Sobon, W. Macherzynski, P. Paletko, K. Grodecki, K. M. Abramski, Mode-locking in er-doped fiber laser based on mechanically exfoliated Sb_2Te_3 saturable absorber, Opt. Mater. Express 4 (1) (2014) 1–6. doi:10.1364/OME.4.000001.

[11] C. Moisset, R.-N. Verrone, A. Bourgade, G. T. Zeweldi, M. Minissale, L. Gallais, C. Perrin-Pellegrino, H. Akhouayri, J. Lumeau, J.-Y. Natoli, K. Iliopoulos, Giant ultrafast optical nonlinearities of annealed Sb_2Te_3 layers, Nanoscale Adv. 2 (2020) 1427–1430. doi:10.1039/C9NA00796B.

[12] D. Coiras, R.-N. Verrone, A. Campos, M. Cabié, L. Gallais, M. Minissale, J. Lumeau, J.-Y. Natoli, K. Iliopoulos, Laser annealing of Sb_2Te_3 2d layers towards nonlinear optical applications, Optics 3 (3) (2022) 234–242. doi:10.3390/opt3030023.

[13] H. W. Liu, H. T. Yuan, N. Fukui, L. Zhang, J. F. Jia, Y. Iwasa, M. W. Chen, T. Hashizume, T. Sakurai, Q. K. Xue, Growth of Topological Insulator Bi_2Te_3 Ultrathin Films on Si(111) Investigated by Low-Energy Electron Microscopy, Crystal Growth & Design 10 (10) (2010) 4491–4493. doi:10.1021/cg1007457.

[14] S. Borisova, J. Krumrain, M. Luysberg, G. Mussler, D. Grützmacher, Mode of Growth of Ultrathin Topological Insulator Bi_2Te_3 Films on Si (111) Substrates, Crystal Growth & Design 12 (12) (2012) 6098–6103. doi:10.1021/cg301236s.

[15] M. Rimoldi, R. Cecchini, C. Wiemer, A. Lamperti, E. Longo, L. Nasi, L. Lazzarini, R. Mantovan, M. Longo, Epitaxial and large area Sb_2Te_3 thin films on silicon by MOCVD, RSC Advances 10 (34) (2020) 19936–19942. doi:10.1039/D0RA02567D.

[16] S. Kim, S. Lee, J. Woo, G. Lee, Growth of Bi_2Se_3 topological insulator thin film on Ge(1 1 1) substrate, Applied Surface Science 432 (2018) 152–155.

[17] D. Kong, W. Dang, J. J. Cha, H. Li, S. Meister, H. Peng, Z. Liu, Y. Cui, Few-Layer Nanoplates of Bi_2Se_3 and Bi_2Te_3 with Highly Tunable Chemical Potential, Nano Letters 10 (6) (2010) 2245–2250. doi:10.1021/nl101260j.

[18] Z. Zeng, T. A. Morgan, D. Fan, C. Li, Y. Hirono, X. Hu, Y. Zhao, J. S. Lee, J. Wang, Z. M. Wang, S. Yu, M. E. Hawkridge, M. Benamara, G. J. Salamo, Molecular beam epitaxial growth of Bi_2Te_3 and Sb_2Te_3 topological insulators on GaAs(111) substrates: a potential route to fabricate topological insulator p-n junction, AIP Advances 3 (7) (2013) 072112. doi:10.1063/1.4815972.

[19] R. Sultana, G. Gurjar, S. Patnaik, V. P. S. Awana, Crystal growth and characterization of bulk Sb_2Te_3 topological insulator, Materials Research Express 5 (4) (2018) 046107. doi:10.1088/2053-1591/aabc33.

[20] C. Wang, Q. Wang, L. Chen, X. Xu, Q. Yao, Electrodeposition of Sb_2Te_3 films on Si(100) and ag substrates, Electrochemical and Solid-State Letters 9 (9) (2006) C147. doi:10.1149/1.2211884.

[21] Y. Saito, P. Fons, A. V. Kolobov, J. Tominaga, Self-organized van der waals epitaxy of layered chalcogenide structures, physica status solidi (b) 252 (10) (2015) 2151–2158. doi:https://doi.org/10.1002/pssb.201552335.

[22] V. Pore, K. Knapas, T. Hatanpää, T. Sarnet, M. Kemell, M. Ritala, M. Leskelä, K. Mizohata, Atomic layer deposition of antimony and its compounds using dechlorosilylation reactions of tris(triethylsilyl)antimony, Chemistry of Materials 23 (2) (2011) 247–254. doi:10.1021/cm102904f.

[23] L. Plucinski, A. Herdt, S. Fahrendorf, G. Bihlmayer, G. Mussler, S. Döring, J. Kampmeier, F. Matthes, D. E. Bürgler, D. Grützmacher, S. Blügel, C. M. Schneider, Electronic structure, surface morphology, and topologically protected surface states of Sb_2Te_3 thin films grown on Si(111), Journal of Applied Physics 113 (5) (2013) 053706. doi:10.1063/1.4789353.

[24] M. Lanius, J. Kampmeier, S. Kölling, G. Mussler, P. Koenraad, D. Grützmacher, Topography and structure of ultrathin topological insulator Sb_2Te_3 films on Si(111) grown by means of molecular beam epitaxy, Journal of Crystal Growth 453 (2016) 158–162. doi:https://doi.org/10.1016/j.jcrysgro.2016.08.016.

[25] E. Salomon, M. Minissale, F. R. Lairado, S. Coussan, P. Rousselot-Pailley, F. Dulieu, T. Angot, Pyrene adsorption on a ag(111) surface, The Journal of Physical Chemistry C 125 (20) (2021) 11166–11174. doi:10.1021/acs.jpcc.1c01350.

[26] M. Minissale, E. Salomon, F. Pappalardo, C. Martin, M. Muntwiler, T. Angot, G. Le Lay, The renaissance and golden age of epitaxial dry germanene, Crystals 13 (2) (2023). doi:10.3390/cryst13020221.

[27] M. Scrocco, X-ray and electron-energy-loss spectra of Bi, Sb, Te and Bi_2Te_3, Sb_2Te_3 chalcogenides, Journal of Electron Spectroscopy and Related Phenomena 50 (2) (1990) 171–184. doi:https://doi.org/10.1016/0368-2048(90)87061-R.

[28] E. Nolot, C. Sabbione, W. Pessoa, L. Prazakova, G. Navarro, Germanium, antimony, tellurium, their binary and ternary alloys and the impact of nitrogen: An x-ray photoelectron study, Applied Surface Science 536 (2021) 147703. doi:https://doi.org/10.1016/j.apsusc.2020.147703.

[29] B. R. Strohmeier, An esca method for determining the oxide thickness on aluminum alloys, Surface and Interface Analysis 15 (1) (1990) 51–56. doi:https://doi.org/10.1002/sia.740150109.

[30] C. Pauly, G. Bihlmayer, M. Liebmann, M. Grob, A. Georgi, D. Subramaniam, M. R. Scholz, J. Sánchez-Barriga, A. Varykhalov, S. Blügel, O. Rader, M. Morgenstern, Probing two topological surface bands of Sb_2Te_3 by spin-polarized photoemission spectroscopy, Phys. Rev. B 86 (2012) 235106. doi:10.1103/PhysRevB.86.235106.

[31] Y. Jiang, Y. Y. Sun, M. Chen, Y. Wang, Z. Li, C. Song, K. He, L. Wang, X. Chen, Q.-K. Xue, X. Ma, S. B. Zhang, Fermi-level tuning of epitaxial Sb_2Te_3 thin films on graphene by regulating intrinsic defects and substrate transfer doping, Phys. Rev. Lett. 108 (2012) 066809. doi:10.1103/PhysRevLett.108.066809.